A Quasi-Zero-Stiffness-Based Sensor System in Vibration Measurement

XiuTing Sun, XingJian Jing, *Member, IEEE*, Jian Xu, and Li Cheng

***Abstract*—Quasi-zero-stiffness (QZS) systems have been extensively studied and used as a useful vibration isolation device. In this paper, the feasibility of the application of a QZS system for vibration measurement is investigated. The structural parameters of the QZS system are first analyzed to ensure that the system is staying at stable equilibriums. Comparisons of the absolute motion of a general and typical vibration platform (e.g., a moving vehicle body) and the motion signal measured from the QZS system attached are then conducted to show the effectiveness of the method under different base excitations. Moreover, the case under which the QZS-based sensor system may not behave well is also studied and potential solutions are discussed. The QZS vibration system is shown to be a useful device for absolute displacement measurement in vibration control systems particularly for moving platforms compared with the exciting methods and would benefit a wide range of engineering practices.**

***Index Terms*—Absolute motion, predeformation spring, quasi-zero-stiffness (QZS) system, vibration sensor.**

I. Introduction

THE STATE measurement for a dynamic system is always a critical task in various engineering practice for system identification, control and filter design, etc. [1]–[13]. Many active vibration control methods for moving platforms (e.g., vehicle suspension, instrument protection in ships or unmanned aerial vehicles (UAVs), etc.) usually require accurate measurement of full system states with respect to a global coordinate system for better performance in vibration suppression [5], [6]. A variety of sensors have been introduced in previous research works for mechatronics systems [14], [15]. Accelerometers are often used to measure the absolute acceleration of a dynamic system, while the absolute displacement of the system would not be straightforward and accurate to measure in moving platforms. For measurement of the absolute displacement or location, although some advanced measurement technologies could be applied, for example, inertial sensors [16], radar or laser technologies [17]–[20], etc., accuracy, installation, or development cost would be realistic issues. To circumvent these burdens, some output feedback control methods could be applied with a dynamic filtering system designed to estimate those unmeasured states [21]–[29] or some existing algorithms (e.g., integration) can directly be used to obtain the unmeasured states (e.g., displacement) from the measured ones (e.g., acceleration). However, these would incur the other problems to the controlled system, e.g., time delay. For the case of using acceleration feedback control with time delay [30], [31], the controlled system would be referred to as a neutral delayed differential equation in the literature, in which it is known that the time delay could easily deteriorate the robustness of the dynamic system and bring complexity for theoretical analysis [32], [33]. Even though time delay could benefit the vibration control when the absolute displacement is used in the feedback control for some cases [30]–[35], the value of the time delay should usually be set in some critical ranges. However, the filtering methods mentioned earlier can often introduce time delay to feedback signals more than what is desired [34], [35].

To conveniently and accurately measure the absolute displacement for vibration control in moving platforms such as vehicle suspension systems or instrument protection in ships or UAVs, etc., a novel quasi-zero-stiffness (QZS)-based sensor system is proposed in this study. The idea comes from the QZS vibration isolator (QZS-VI) which can isolate the vibration from the base structure [36]–[39]. This kind of isolators is often connected to the base by two horizontal springs and a vertical spring and has many advantages such as small static displacement, small dynamic stiffness, and low natural frequency. Because of the remarkable isolation effect of the QZS-VI, the relative motion between the QZS system and the base structure can be close to the absolute motion of the base structure below. In order to decrease the error between the relative motion and absolute motion aforementioned, the stiffness characteristics and geometric parameters of the QZS system should be properly analyzed and designed [36]–[39]. This paper utilizes the isolation characteristic of the QZS system to approximately obtain the absolute displacement of moving platforms. The QZS-based sensor system is easy to design and convenient to implement in practice and no time delay problems would be incurred. It is shown that the QZS-based vibration sensor is very effective for absolute displacement measurement of moving platforms in a large frequency range under different excitation signals.

This paper is organized as follows. The novel QZS-based sensor system is introduced in Section II. Then, the equilibrium position and static stability of the system are analyzed to

Manuscript received July 3, 2013; accepted November 27, 2013. Date of publication January 2, 2014; date of current version May 2, 2014. This work was supported in part by the National Science Foundation of China projects under No. 61374041, Ref. 11272326, and No. 11032009; in part by a General Research Fund Project of the Hong Kong Research Grants Council under Ref. 517810; and in part by the Internal Research Grants of Hong Kong Polytechnic University. *(Corresponding author: X. J. Jing.)*

X. T. Sun is with the Department of Mechanical Engineering, Hong Kong Polytechnic University, Hong Kong, and also with Tongji University, Shanghai 200092, China.

X. J. Jing and L. Cheng are with the Department of Mechanical Engineering, Hong Kong Polytechnic University, Hong Kong, and also with the Hong Kong Polytechnic University Shenzhen Research Institute, Shenzhen, China (e-mail: mmjxj@polyu.edu.hk; xingjian.jing@gmail.com).

J. Xu is with the School of Aerospace Engineering and Applied Mechanics, Tongji University, Shanghai 200092, China.

Digital Object Identifier 10.1109/TIE.2013.2297297

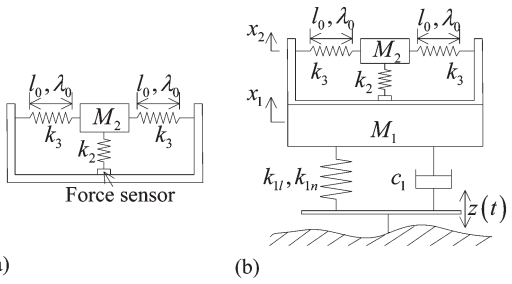

Fig. 1. Scheme of the QZS-based sensor on a moving platform. (a) QZS-based sensor. (b) Overall vibration system.

TABLE I
STRUCTURAL PARAMETERS OF THE QZS-BASED VIBRATION SENSOR

Symbol	Structural parameters	Unit
k_2	vertical spring stiffness	N/m
k_3	horizontal spring stiffness	N/m
M_2	mass of vibration sensor	kg
l_0	origin length of horizontal spring	m
c_2	structural damping	N·s/m
λ_1	initial deformation of horizontal spring	m
λ_0	pre-deformation of horizontal spring	m

show the effect of structure parameters on linear and nonlinear responses. The dynamic responses of the QZS-based sensor system are given under different base excitations in Section IV. Section V shows the influence of the QZS-based sensor system on the host vibration system. An example is illustrated in Section VI. Finally, a conclusion is drawn.

II. DESIGN OF THE QZS-BASED SENSOR SYSTEM

The QZS-based sensor proposed in this paper is a single-degree-of-freedom (DOF) system attached to a moving platform, as shown in Fig. 1. The sensor part is a QZS-based system which is made of a small mass, two horizontal prepressing springs, and a vertical spring. The original length of the horizontal spring is l_0, and its predeformation is λ_0. The stiffness of the vertical spring is k_2, and that of the horizontal spring is k_3. The vertical spring could be connected with a force sensor or else to measure the relative displacement between M_1 and M_2. The springs of the vibration sensor system are fixed on a frame. The structural parameters of the QZS vibration sensor are listed in Table I.

In Fig. 1(b), the mass–spring–damper vibration system subjected to a base excitation can be widely found in engineering practice (e.g., a quarter-vehicle suspension model). Utilizing the QZS-based sensor approximately measures the absolute displacement of the vibration platform by measuring the relative displacement of the major mass, i.e., M_2, in the QZS system (many methods are available for this measurement, e.g., using a force sensor, as shown in Fig. 1). The QZS system is connected to the base by a spring with linear stiffness k_{1l} and a nonlinear stiffness k_{1n} and a damping c_1. From Fig. 1(b), the absolute displacement of M_1 is $x_1(t)$, the absolute displacement of M_2 is $x_2(t)$, and the displacement input from the base is $z(t)$. The structural parameters of the system and kinematical variables are listed in Table II.

TABLE II
STRUCTURAL PARAMETERS AND KINEMATICAL VARIABLES OF THE SYSTEM

Symbol	Structural parameters	Unit
k_{1l}	linear stiffness of the quarter-vehicle model	N/m
k_{1n}	nonlinear stiffness of the quarter-vehicle model	N/m
c_1	damping coefficient of vehicle	N·s/m
M_1	mass of vehicle	kg
$z(t)$	excitation from base	m
$x_1(t)$	absolute motion of vehicle	m
$x_2(t)$	absolute motion of vibration sensor	m
$u_1(t)$	relative motion of vehicle and base	m
$u_2(t)$	relative motion of vibration sensor and vehicle	m
ω_i	Frequency of multi-periodic base input	rad/s
z_i	amplitude of multi-periodic base displacement input	m
ω	frequency of single-periodic base input and responses	rad/s
z_0	amplitude of single-periodic base input	m

In practice, in order to suppress the vibration of the platform, different forms of active or passive control methods are studied [5], [6], [23], [24], which usually require knowing the absolute displacement of the platform for a better performance. However, as mentioned before, the existing methods often have obvious limitations to achieve the absolute vibrating displacement of the platform, and existing displacement sensors can usually measure the relative motion between the body and base for the moving platform.

III. STATIC CHARACTERISTICS

A. Modeling

Based on the model in Fig. 1(b), the equations of the vehicle and vibration sensor can be established by a Lagrange equation. The kinetic energy of the system can be written as

$$T = \frac{1}{2}M_1\dot{x}_1^2 + \frac{1}{2}M_2\dot{x}_2^2 \tag{1}$$

and the potential energy as

$$V = \frac{1}{2}k_{1l}(x_1 - z)^2 + \frac{1}{4}k_{1n}(x_1 - z)^4 + \frac{1}{2}k_2(x_2 - x_1)^2 + k_3\left(l_0 - \sqrt{(l_0 - \lambda_0)^2 + (x_2 - x_1)^2}\right)^2. \tag{2}$$

For the two generalized coordinates x_1 and x_2, according to the Lagrange equation, the dynamic equation of the system is

$$\begin{aligned} \frac{d}{dt}\frac{\partial(T-V)}{\partial\dot{x}_1} - \frac{\partial(T-V)}{\partial x_1} &= -c_1(\dot{x}_1 - \dot{z}) \\ \frac{d}{dt}\frac{\partial(T-V)}{\partial\dot{x}_2} - \frac{\partial(T-V)}{\partial x_2} &= -c_2\dot{x}_2. \end{aligned} \tag{3}$$

Substituting the kinetic energy and potential energy into (1) and (2), the dynamic of the system is

$$\begin{aligned} &M_1\ddot{x}_1 + k_{1l}(x_1 - z) + k_{1n}(x_1 - z)^3 + c_1(\dot{x}_1 - \dot{z}) \\ &\quad + 2k_3\frac{(x_2 - x_1)\left[l_0 - \sqrt{(l_0 - \lambda_0)^2 + (x_2 - x_1)^2}\right]}{\sqrt{(l_0 - \lambda_0)^2 + (x_2 - x_1)^2}} \\ &\quad - k_2(x_2 - x_1) - k_2(x_2 - x_1) = 0 \end{aligned} \tag{4}$$

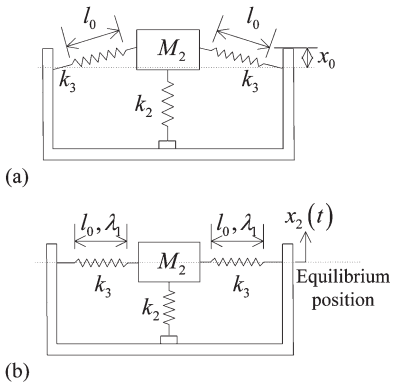

Fig. 2. Assembly process of the QZS vibration sensor. (a) Position before assembling mass. (b) Equilibrium position of the vibration sensor.

$$M_2\ddot{x}_2 + c_2\dot{x}_2 + k_2(x_2 - x_1) - 2k_3\frac{(x_2 - x_1)\left[l_0 - \sqrt{(l_0 - \lambda_0)^2 + (x_2 - x_1)^2}\right]}{\sqrt{(l_0 - \lambda_0)^2 + (x_2 - x_1)^2}} = 0. \tag{5}$$

The force signal obtained by the force sensor on the vertical spring is F which can be written as

$$F = k_2(x_2 - x_1). \tag{6}$$

From (6), the force is closer to the value of k_2x_1 for a smaller amplitude of x_2, i.e., $F \approx -k_2x_1$ for an ideal zero-stiffness system. This means that the QZS system can approximately measure the displacement of the base platform and the accuracy depends mainly on the isolation effect of the QZS system.

B. Static Equilibrium Position

Fig. 2 shows the assembly process of the QZS-based vibration sensor. Fig. 1(a) shows the initial state of the springs. There is x_0 from the mass to equilibrium position. To guarantee the symmetrical characteristic of the vibration, the two springs with stiffness k_3 should be horizontal after assembling the mass M_2 and the equilibrium position of the QZS vibration sensor should be at the horizontal level, as indicated in Fig. 2(b).

By principle of virtual displacement, the distance x_0 and mass M_2 should satisfy the following condition:

$$\frac{\partial\left\{M_2gx_0 + k_3\left[\sqrt{l_0^2 - x_0^2} - l_0\right]^2 + \frac{1}{2}k_2x_0^2\right\}}{\partial x_0} = 0. \tag{7}$$

Then, the initial deformation of the horizontal springs is

$$\lambda_1 = l_0 - \sqrt{l_0^2 - x_0^2}. \tag{8}$$

The vertical spring can ensure a stable equilibrium [Fig. 2(b)].

In the assembly of the QZS system, to ensure that the mass M_2 should reach the horizontal equilibrium position, (7) and (8) should be satisfied. The relationship between initial deformation λ_1 and mass M_2 is an implicit function but the value of initial deformation can be obtained easily for a value of mass M_2.

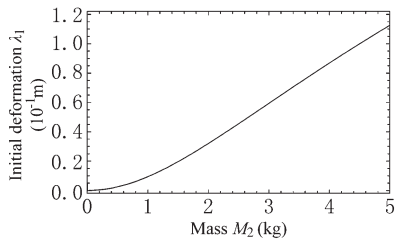

Fig. 3. Initial deformation λ_1 of the horizontal spring due to a different mass M_2.

Fig. 3 is the initial deformation of the horizontal spring λ_1 for a different mass M_2 under $l_0 = 0.5$ and $k_3 = 300$. For a heavier mass, i.e., M_2, the horizontal spring is more compressed. After assembling the mass M_2 which will induce the initial deformation λ_1 of the horizontal spring, the two horizontal springs should be compressed to a desired value λ_0 for better vibration isolation.

C. Stiffness of the QZS-Based Vibration Sensor

Form the previous analysis, the initial deformation increases with the mass in the QZS vibration sensor increasing. However, if the coefficients of the predeformation and mass are improperly changed, the equilibrium position of the QZS vibration sensor is unstable, which can induce faulty measurement. Thus, to maintain the stability of equilibrium position, the predeformation λ_0 and other parameters of the vibration sensor are required to stay in a reasonable range.

Utilizing the relative vibration as the variables, the dynamic equation can be expressed as

$$M_1\ddot{u}_1 + k_{1l}u_1 + k_{1n}u_1^3 + c_1\dot{u}_1 - k_2u_2 + 2k_3\frac{u_2\left[l_0 - \sqrt{(l_0 - \lambda_0)^2 + u_2^2}\right]}{\sqrt{(l_0 - \lambda_0)^2 + u_2^2}} = -M_1\ddot{z} \tag{9}$$

$$M_2(\ddot{u}_1 + \ddot{u}_2) + c_2(\dot{u}_1 + \dot{u}_2) + k_2u_2 - 2k_3\frac{u_2\left[l_0 - \sqrt{(l_0 - \lambda_0)^2 + u_2^2}\right]}{\sqrt{(l_0 - \lambda_0)^2 + u_2^2}} = -c_2\dot{z} - M_2\ddot{z} \tag{10}$$

where $u_1 = x_1 - z$ is the relative motion of the platform to the base and $u_2 = x_2 - x_1$ is the relative motion of mass M_2 to the platform.

The applied force of the QZS vibration sensor is

$$f = k_2u_2 - 2k_3\frac{u_2\left[l_0 - \sqrt{(l_0 - \lambda_0)^2 + u_2^2}\right]}{\sqrt{(l_0 - \lambda_0)^2 + u_2^2}}. \tag{11}$$

The applied force can be expanded to the Taylor series expansion, which approximately reflects the static characteristics and simplifies the calculation of the sensor. The third-order Taylor series expansion is employed as follows:

$$f = \left(k_2 + 2k_3 - \frac{2k_3l_0}{l_0 - \lambda_0}\right)u_2 + \frac{k_3l_0}{(l_0 - \lambda_0)^3}u_2^3 + o\left(u_2^5\right). \tag{12}$$

In Fig. 4, the values of the applied force expanded by the third-order Taylor series are close to the original expression

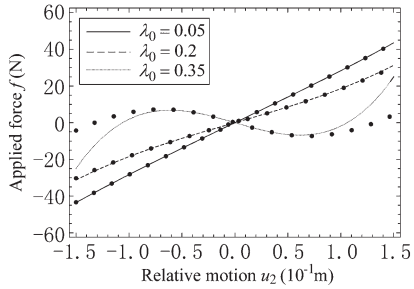

Fig. 4. Comparison of the applied force of (lines) (11) and (dots) the third-order Taylor expansion as (12) for different λ_0's for $k_2 = 300$, $k_3 = 100$, and $l_0 = 0.5$.

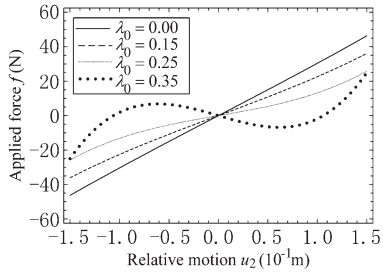

Fig. 5. Applied force for different λ_0's for $k_2 = 300$, $k_3 = 100$, and $l_0 = 0.5$.

of (9). Thus, the dynamical equation of the two-freedom isolator is

$$M_1\ddot{u}_1 + k_{1l}u_1 + k_{1n}u_1^3 + c_1\dot{u}_1 - k_3\frac{l_0}{(l_0-\lambda_0)^3}u_2^3 - \left(k_2 + 2k_3 - \frac{2k_3l_0}{l_0-\lambda_0}\right)u_2 = -M_1\ddot{z} \quad (13)$$

$$M_2(\ddot{u}_1+\ddot{u}_2) + c_2(\dot{u}_1+\dot{u}_2) + \frac{k_3l_0}{(l_0-\lambda_0)^3}u_2^3 + \left(k_2 + 2k_3 - \frac{2k_3l_0}{l_0-\lambda_0}\right)u_2 = -c_2\dot{z} - M_2\ddot{z} \quad (14)$$

where the base excitation is given by $z(t) = z_0\cos\omega t$.

When $k_2 = 300$, $k_3 = 100$, and $l_0 = 0.5$, the curves of the Taylor series expansion (12) of the applied force are shown in Fig. 5 for different values of predeformation λ_0. In Fig. 5, the gradient of the applied force f deceases with the increasing of λ_0 and can be zero for the proper value of λ_0 at $u_2 = 0$. From the dynamical equation, the closer the value of the gradient of the applied force to the zero, the more similar the relative motion u_2 and the absolute motion of the platform x_1. Therefore, from (12), the gradient of the applied force at $u_2 = 0$ equals to zero when $k_2 + 2k_3 - 2k_3l_0/(l_0-\lambda_0) = 0$, which means when $\lambda_0 = k_2l_0/(k_2+2k_3)$, the linear part of the applied force equals zero and then $f = k_3l_0u_2^3/(l_0-\lambda_0)^3$.

IV. Dynamic Response Under Different Excitations

A. Single-Frequency Excitation

From the analysis of the applied force f, the QZS device realizes the vibration isolation between the mass M_1 and mass M_2. Because of the QZS, the amplitude of the relative motion u_2 is close to the amplitude of the absolute motion x_1, i.e., $u_2 \approx -x_1$. The closer the linear part of the QZS system to zero, the smaller the difference between u_2 and $-x_1$. The response of the moving platform and the corresponding signal measured are studied to show that the QZS-based sensor is effective and useful for vibration measurement. The relative motions of the overall two-DOF vibration system are defined as $u_1(t) = a_1\cos\omega t + b_1\sin\omega t$ and $u_2(t) = a_2\cos\omega t + b_2\sin\omega t$, where a_1, b_1, a_2, and b_2 are the values of the basic harmonic solutions of (13) and (14).

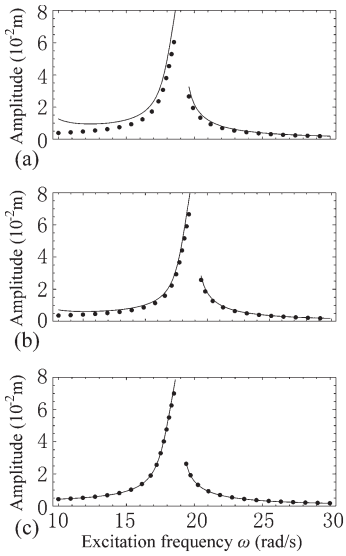

Fig. 6. Comparison of the (lines) amplitude of relative motion u_2 and (dots) absolute motion x_1 for (a) $\lambda_0 = 0.25$, (b) $\lambda_0 = 0.28$, and (c) $\lambda_0 = 0.3$.

The absolute motion of the vibration platform is $x_1 = u_1 + z$. For the relative motion solution $u_1 = x_1 - z$, its expression is $x_1(t) = (a_1+z_0)\cos\omega t + b_1\sin\omega t$. Similarly, the expression of the relative motion solution u_2 is $u_2(t) = a_2\cos\omega t + b_2\sin\omega t$. These expressions are substituted into (13) and (14) and the coefficients of the sin and cos functions of the resulting equations should be zero, and then, the amplitude of the absolute motions and relative motions can be obtained. The amplitudes of the absolute and relative motions are $[(a_1+z_0)^2 + b_1^2]^{1/2}$ and $(a_2^2+b_2^2)^{1/2}$, respectively. The frequency–amplitude curves of x_1 and u_2 are shown in Fig. 6. The phase of the absolute motion x_1 is defined as θ_1, and that of u_2 is θ_2, as given by $\theta_1 = \arctan[-b_1/(a_1+z_0)]$ and $\theta_2 = \arctan(-b_2/a_2)$. The phase responses are shown in Fig. 7.

Because the predeformation parameter λ_0 is the most critical factor affecting the vibration isolation performance of the QZS system [36]–[39] and, thus, the most crucial factor influencing the accuracy of the sensor system compared with the other structural parameters, the results in what follows only indicate the accuracy performance with different λ_0 values while the other parameters are given just for example, satisfying that 1) λ_0 is around $k_2l_0/(k_2+2k_3)$ (such that the linear stiffness in (12) is zero) and 2) $M_2 \ll M_1$ [such that the accuracy of the sensor can be guaranteed in a larger frequency range and no additional coupling resonance frequency is incurred (see Section V)].

Fig. 6 shows the frequency amplitude response, and Fig. 7 shows the phases of relative motion u_2 and absolute motion

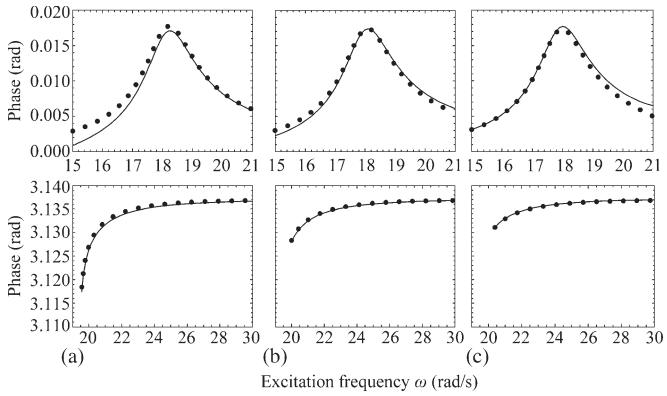

Fig. 7. Phases of the (lines) relative motion u_2 and (dots) absolute motion x_1 for (a) $\lambda_0 = 0.25$, (b) $\lambda_0 = 0.28$, and (c) $\lambda_0 = 0.3$.

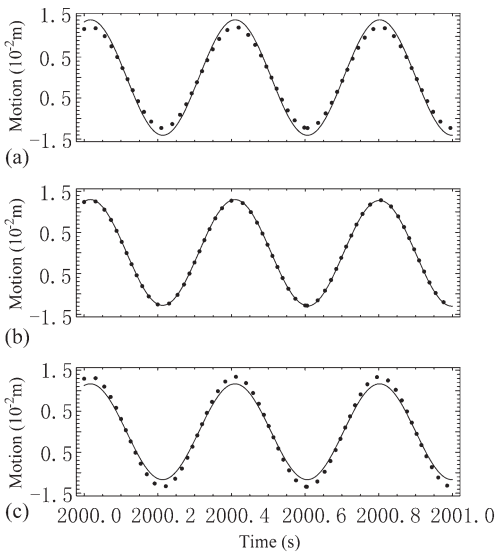

Fig. 8. Time series of the (lines) relative motion u_2 and (dots) absolute motion $-x_1$ for (a) $\lambda_0 = 0.28$, (b) $\lambda_0 = 0.3$, and (c) $\lambda_0 = 0.32$.

x_1 for different λ_0 values with $M_1 = 15$, $M_2 = 1.44$, $l_0 = 0.5$, $k_{1l} = 5000$, $k_{1n} = 100\,000$, $k_2 = 300$, $k_3 = 100$, $c_1 = 2$, and $c_2 = 1$, $z_0 = 0.003$. For $\lambda_0 = 0.25$ and $\lambda_0 = 0.28$, the relative motion has more deviation from the absolute motion and the deviation is obvious at low frequency. For $\lambda_0 = 0.3$, the amplitude of u_2 is very close to x_1 in a wider frequency range.

Fig. 8 is the time-series of u_2 and $-x_1$. With appropriate value of pre-deformation λ_0, there is $u_2 = x_2 - x_1 \approx -x_1$ due to $x_2 \approx 0$. The deviation from the best value of pre-deformation λ_0 induces the error between u_2 and $-x_1$.

From Fig. 9, the relative error of the two amplitudes extremely depends on the predeformation. With the decreasing of predeformation λ_0, the relative error of amplitude between the relative motion u_2 and absolute motion $-x_1$ increases. The error is very close to zero for small base excitation as $\lambda_0 = 0.3$. Also, the larger value of the amplitude of base excitation z_0 induces a slightly larger proportional error of the two amplitudes due to the high-order nonlinear truncation in numerical computation.

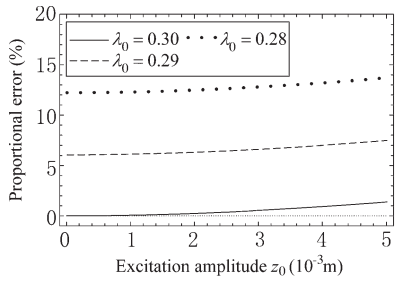

Fig. 9. Proportional error between the amplitude of the relative motion u_2 and absolute motion $-x_1$ under different amplitudes of base excitation z_0 and predeformation λ_0.

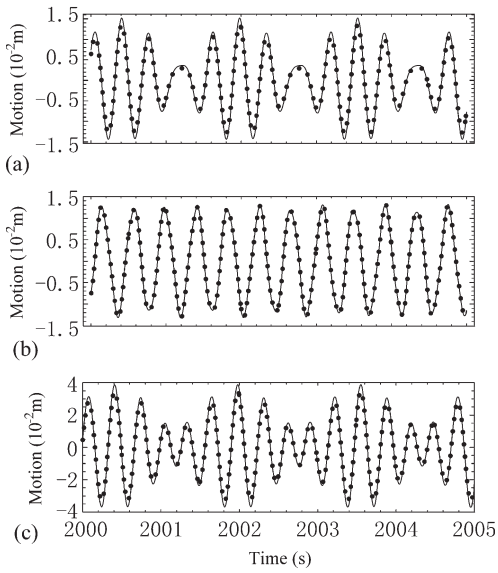

Fig. 10. Time series of (solid) u_2 and (dotted) $-x_1$ for multifrequency excitation of different values of parameters (a) $\lambda_0 = 0.28$, $z_0 = 0.002$, $z_1 = 0.001$, $\omega_0 = 16$, $\omega_1 = 20$, $z_2 = z_3 = \cdots = 0$; (b) $\lambda_0 = 0.3$, $z_0 = 0.004$, $z_1 = 0.003$, $\omega_0 = 15$, $\omega_1 = 38$, $z_2 = z_3 = \cdots = 0$; (c) $\lambda_0 = 0.28$, $z_0 = 0.002$, $z_1 = 0.001$, $z_2 = 0.004$, $\omega_0 = 16$, $\omega_1 = 21$, $\omega_2 = 21$, $z_3 = z_4 = \cdots = 0$.

B. Multifrequency Excitation

The QZS system also performs well under multifrequency excitation. For a base excitation $z = \sum z_i \cos(\omega_i t + \varphi_i)$, the responses of u_2 and $-x_1$ are shown for different values of excitation amplitude. In simulations, all phase angles φ_i's are set to zero.

Fig. 10 shows the time series of the relative motion and the absolute motion for different cases. The relative motion u_2 is very close to $-x_1$. The result shows that the amplitudes of the two motions are very approximate and their error becomes smaller for the appropriate value of predeformation λ_0. Also, the phases of the two motions are observed to be similar to each other for different parameters. Therefore, under the multifrequency base excitation, the signal measured by the QZS-based sensor can also reflect the absolute motion of the motion of the vibrating platform.

C. Random Excitation

Considering random excitations, the mean value of the random input signal is set to zero, the unbiased variance is $0(10^{-3})$,

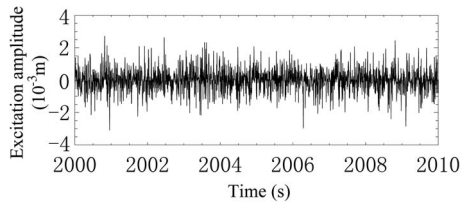

Fig. 11. Random input signal.

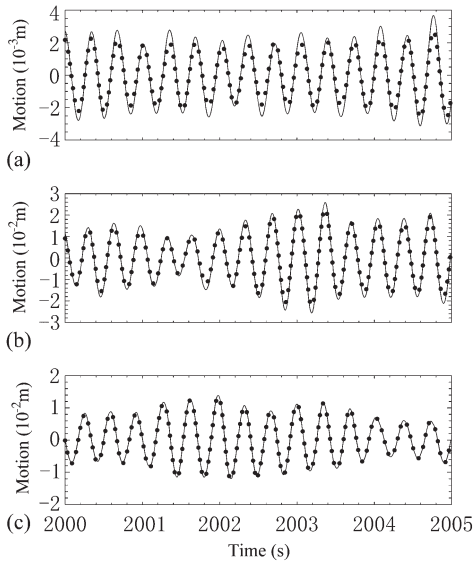

Fig. 12. Comparison of (lines) u_2 and (dots) $-x_1$ under random input for (a) $\lambda_0 = 0.26$, (b) $\lambda_0 = 0.28$, and (c) $\lambda_0 = 0.3$.

and the frequency range of the random signal is set into the range of [15, 65] rad/s, which is shown partially in Fig. 11.

In the simulations, the input signals are different in each simulation, satisfying the conditions aforementioned. For different values of predeformation, i.e., $\lambda_0 = 0.26, 0.28,$ and 0.3, the comparisons between the relative motion u_2 and absolute motion $-x_1$ are shown in Fig. 12. For $\lambda_0 = 0.3$, the relative motion u_2 is very close to $-x_1$. The relative motion u_2 can reflect the absolute motion, and the error of the two motions decreases as the linear part is near to zero by adjusting the predeformation λ_0.

From the analysis and numerical simulation aforementioned, it can be concluded that the QZS-based sensor is effective for different input excitations including periodic and random base excitations. The predeformation λ_0 has huge impact on the error between the relative motion u_2 and absolute motion $-x_1$, and the error can be designed to approximately zero. Different methods can be used to measure the relative motion u_2, which is an approximation of x_1. For example, when applying the force sensor on the spring k_2, the force signal measured is $k_2 u_2$, and the absolute displacement x_1 can be approximately and easily obtained from this force signal by dividing the constant $-k_2$.

V. Potential Influence by the QZS-Based Vibration Sensor

Although the QZS-based sensor can approximately measure the absolute motion of the moving platform under different base excitations, it could also induce a problem to the system.

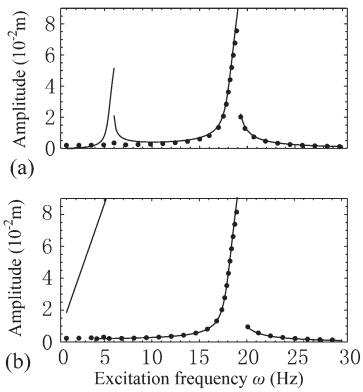

Fig. 13. Magnitudes of (solid) u_2 and (dotted) x_1 for (a) $\lambda_0 = 0.28$ and (b) $\lambda_0 = 0.3$.

When the QZS-based sensor is attached to the moving platform, the overall system could become a two-freedom vibration system. There is another resonant frequency therefore induced. The resonant frequency of the original system is $\omega_1 = (k_{1l}/M_1)^{1/2}$ while the resonant frequencies of the two-freedom system are determined by the linear part of the dynamic (13) and (14) as

$$k_{1l}\beta\Omega^4 - (k_{1l} + \beta)\Omega^2 + M_1 M_2 - M_2\beta = 0 \qquad (15)$$

where $\beta = k_2 + 2k_3 - 2k_3 l_0/(l_0 - \lambda_0)$ and Ω is the resonant frequency of the coupled system. From the analysis of stability, the parameter β cannot be negative. For $\beta > 0$, the resonant frequencies are

$$\Omega_{1,2} = \sqrt{\frac{k_{1l} + \beta \pm \sqrt{(k_{1l} + \beta)^2 - 4(M_1 M_2 - M_2\beta)}}{2k_{1l}\beta}}. \qquad (16)$$

For $\beta = 0$, one of the two resonant frequencies equals zero and the other one equals $(k_{1l}/M_1)^{1/2}$. However, for the nonlinearity of the vibration system, there are a resonant peak and a jump phenomenon in the low-frequency range even for $\beta = 0$.

Fig. 13 shows the frequency responses for u_2 and x_1. There are a resonant peak and a jump phenomenon at the low-frequency range where the amplitude of the relative motion u_2 cannot represent the amplitude of the absolute motion x_1. For the low-frequency base excitations, the signal measured by the QZS-based sensor will lose the accuracy and validity. However, in this case, a low-frequency antiresonance isolation such as a lever-type isolator [39] could be applied for performance improvement, which will be investigated in a future study.

Although it can induce a new resonant frequency by coupling with the QZS-based sensor, the induced resonant peak could be very small if the mass of the sensor is small relative to the platform mass and, thus, could be neglected.

VI. Application of the QZS-Based Vibration Sensor

One straightforward application of the proposed QZS-based sensor is for vibration control. There are many results for semi-active or active feedback control for vibration suppression, which rely strictly on the absolute state feedback (e.g., position, velocity, or acceleration) [7]–[10]. However, compared with

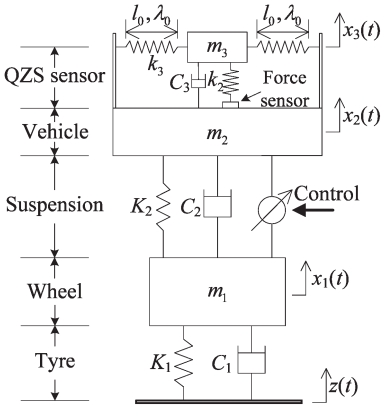

Fig. 14. Use of QZS sensor for feedback control in a quarter-vehicle system.

measuring the absolute motion of the vibrating system, it is usually much easier to obtain the relative motion between the vibration platform and vibration base. Therefore, this paper provides a novel and convenient method for measurement of absolute motion, which can directly be used as feedback signal in these semi-/active vibration control systems. As an example, consider the quarter-vehicle suspension system in [7]–[10] shown in Fig. 14. The structure parameters in this system $x_1(t)$, $x_2(t)$, and $x_3(t)$ represent the absolute displacements of the wheel m_1, vehicle m_2, and QZS system m_3, respectively; $z(t)$ is the base excitation; K_1 and C_1 are the stiffness and damping of the pneumatic tyre; and K_2 and C_2 are the stiffness and damping of the suspension system. In the QZS-based sensor, k_2 and k_3 represent the stiffness of the vertical spring and horizontal spring, C_3 is the damping of the vertical spring k_2, l_0 is the original length, and λ_0 is the predeformation of the horizontal springs.

The system model with feedback control is given as

$$m_1\ddot{x}_1 + K_1(x_1 - z) + K_2(x_1 - x_2) + C_1(\dot{x}_1 - \dot{z}) + C_2(\dot{x}_1 - \dot{x}_2) = g \tag{17}$$

$$m_2\ddot{x}_2 + K_2(x_2 - x_1) + C_2(\dot{x}_2 - \dot{x}_1) + C_3(\dot{x}_2 - \dot{x}_3) + \left(k_2 + 2k_3 - \frac{2k_3 l_0}{l_0 - \lambda_0}\right)(x_2 - x_3) + \frac{k_3 l_0 (x_2 - x_3)^3}{(l_0 - \lambda_0)^3} = -g \tag{18}$$

$$m_3\ddot{x}_3 + C_3(\dot{x}_3 - \dot{x}_2) + \left(k_2 + 2k_3 - \frac{2k_3 l_0}{l_0 - \lambda_0}\right)(x_3 - x_2) + \frac{k_3 l_0 (x_3 - x_2)^3}{(l_0 - \lambda_0)^3} = 0 \tag{19}$$

where g is the control input. The signal measured by the force sensor in the QZS-based sensor is $k_2(x_2 - x_3)$, used directly as the feedback signal. Thus, it can be written as $g = \alpha(x_2 - x_3)$ where α is the control gain. Simplifying the dynamic equations gives

$$m_1\ddot{u}_1 + K_1 u_1 - K_2 u_2 + C_1\dot{u}_1 - C_2\dot{u}_2 = \alpha u_3 - m_1\ddot{z} \tag{20}$$

$$m_2(\ddot{u}_1 + \ddot{u}_2) + K_2 u_2 + C_2\dot{u}_2 - C_3\dot{u}_3 - \left(k_2 + 2k_3 - \frac{2k_3 l_0}{l_0 - \lambda_0}\right)u_3 - \frac{k_3 l_0 u_3^3}{(l_0 - \lambda_0)^3} = -\alpha u_3 - m_2\ddot{z} \tag{21}$$

$$m_3(\ddot{u}_1 + \ddot{u}_2 + \ddot{u}_3) + C_3\dot{u}_3 + \left(k_2 + 2k_3 - \frac{2k_3 l_0}{l_0 - \lambda_0}\right)u_3 + \frac{k_3 l_0 u_3^3}{(l_0 - \lambda_0)^3} = -m_3\ddot{z} \tag{22}$$

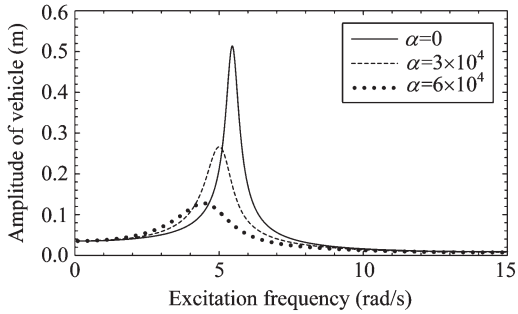

Fig. 15. Frequency–amplitude curves of the vehicle under feedback control.

where u_1, u_2, and u_3 are relative motions given by $u_1 = x_1 - z$, $u_2 = x_2 - x_1$, and $u_3 = x_3 - x_2$ and $z = z_0 \cos\omega t$. The values of different structure parameters are borrowed from [7] as $m_1 = 100$ kg, $m_2 = 1000$ kg, $K_1 = 101.1$ KN $\cdot$ m^{-1}, $K_2 = 42.7$ KN $\cdot$ m^{-1}, $C_1 = 20$ Ns $\cdot$ m^{-1}, $C_2 = 1095$ Ns $\cdot$ m^{-1}, and $z_0 = 0.035$ m. Obviously, the QZS-based sensor acts here to obtain the absolute motion of the vehicle used as feedback signal. In the previous discussions, the parameters of the QZS-based sensor are set as $m_3 = 1$ kg, $k_2 = 300$ N $\cdot$ m^{-1}, $k_3 = 100$ N $\cdot$ m^{-1}, $C_3 = 2$ Ns $\cdot$ m^{-1}, $l_0 = 0.5$ m, and $\lambda_0 = 0.3$ m. Applying the harmonic balance method, the frequency responses with different gain α values are obtained and shown in Fig. 15.

From Fig. 15, the resonant frequency, resonant peak, and amplitude at high frequency can all be reduced, which proves that the feedback control $g = \alpha(x_2 - x_3)$ using the signal obtained by the QZS system as feedback signal is very effective in this vibration control. Note that the relative motion between the QZS system and vehicle is very close to the absolute motion of the vehicle. Therefore, the output of the QZS-based vibration sensor is actually the absolute motion of the system. This shows a very effective and simple method for measuring the absolute motion of a vibration platform in vibration control. First, compared with the results in [7]–[10], the vibration isolation range achieved by the feedback control using the proposed QZS-based sensor is much wider than that with H_∞ control in [7]–[10]. Second, the time delay in signal processing involved in a complicated control process can be greatly reduced with the proposed sensor, because the signal measured by the force sensor of the QZS-based sensor system can directly be used as feedback signal as shown earlier. Third, although the absolute motion of the vehicle body can be obtained by accelerometers [23], [24], further computation process must be involved to obtain the absolute displacement and will inevitably induce time delay and computational error. Displacement sensors usually need a global stationary point. Even compared with laser or ultrasonic sensors for absolute displacement measurement in the aforementioned application, the QZS-based sensor provides the direct reflection on the wheel–ground vibration interaction instead of the ground surface fluctuation (an indirect measurement). Note also that the QZS-based sensor is often much smaller than the vibrating

platform and thus affects little on natural frequency, stiffness, and damping properties of the original system.

From the aforementioned example and discussions, the QZS-based sensor can help achieve excellent vibration control performance with convenient, reliable, and effective absolute displacement measurement. Importantly, the experiments done previously in [39] show that the QZS system has very good performance in vibration isolation, indicating the effectiveness of the novel sensor system in practical application.

VII. Conclusion

This paper has proposed a simple and effective method for measurement of the absolute motion of a moving platform for vibration control and signal processing. A QZS-based sensor system has thus been developed and demonstrated to this aim. The QZS system, which is initially developed in the literature for vibration suppression, is now proposed to act as a vibration sensor which can be used to measure the absolute motion approximately. The design and application of the QZS-based vibration sensor is discussed by adjusting structural parameters in order to achieve a stable and accurate sensor system, considering potential problems. Different base excitations are tested for the novel QZS-based sensor system, which vindicates clearly the effectiveness and potential value of this method in practical applications for different purposes. The example given demonstrates a very practical and successful application of the novel sensor system, showing its obvious advantages and potential value in absolute motion measurement for vibration control, filter design, system identification, etc. Further study will focus on prototyping the novel sensor system and its detailed application issue.

References

[1] A. Benallegue, A. Mokhtari, and L. Fridman, "High-order sliding-mode observer for a quadrotor UAV," *Int. J. Robust Nonlin. Control*, vol. 18, no. 4/5, pp. 427–440, Mar. 2008.

[2] A. J. Calise, N. Hovakimyan, and M. Idan, "Adaptive output feedback control of nonlinear systems using neural networks," *Automatica*, vol. 37, no. 8, pp. 1201–1211, Aug. 2001.

[3] B. Aldiwi and H. K. Khalil, "Robust adaptive output feedback control of nonlinear systems without persistence of excitation," *Automatica*, vol. 33, no. 11, pp. 2025–2032, Nov. 1997.

[4] T. Umeno and Y. Hori, "Robust speed control of DC servomotors using modern two-degrees-of-freedom controller design," *IEEE Trans. Ind. Electron.*, vol. 38, no. 5, pp. 363–368, Oct. 1991.

[5] X. C. Zhu, X. J. Jing, and L. Cheng, "Magnetroheological fluid dampers: A review on structure design and analysis," *J. Intell. Mater. Syst. Struct.*, vol. 23, no. 8, pp. 839–873, Mar. 2012.

[6] X. C. Zhu, X. J. Jing, and L. Cheng, "A magnetorheological fluid embedded pneumatic vibration isolator allowing independently adjustable stiffness and damping," *Smart Mater. Struct.*, vol. 20, no. 8, pp. 085025-1–085025-8, Aug. 2011.

[7] H. Y. Li, X. J. Jing, and H. R. Karimi, "Output-feedback based H_∞ control for vehicle suspension systems with control delay," *IEEE Trans. Ind. Electron.*, vol. 61, no. 1, pp. 436–446, Jan. 2014.

[8] W. C. Sun, Y. Zhao, J. F. Li, L. X. Zhang, and H. J. Gao, "Active suspension control with frequency band constraints and actuator input delay," *IEEE Trans. Ind. Electron.*, vol. 59, no. 1, pp. 530–537, Jan. 2012.

[9] H. Y. Li, H. H. Liu, H. J. Gao, and P. Shi, "Reliable fuzzy control for active suspension systems with actuator delay and fault," *IEEE Trans. Fuzzy Syst.*, vol. 20, no. 2, pp. 342–357, Apr. 2012.

[10] W. C. Sun, H. J. Gao, and O. Kaynak, "Adaptive backstepping control for active suspension systems with hard constraints," *IEEE/ASME Trans. Mechatronics*, vol. 18, no. 3, pp. 1072–1079, Jun. 2013.

[11] X. J. Jing and L. Cheng, "An optimal-PID control algorithm for training feedforward neural networks," *IEEE Trans. Ind. Electron.*, vol. 60, no. 6, pp. 2273–2283, Jun. 2013.

[12] Y. Maeda and M. Iwasaki, "Circle condition-based feedback controller design for fast and precise positioning," *IEEE Trans. Ind. Electron.*, vol. 61, no. 2, pp. 1113–1122, Feb. 2014.

[13] H. Y. Li, J. Y. Yu, C. Hilton, and H. H. Liu, "Adaptive sliding-mode control for nonlinear active suspension vehicle systems using T-S fuzzy approach," *IEEE Trans. Ind. Electron.*, vol. 60, no. 8, pp. 3328–3338, Aug. 2013.

[14] R. C. Luo, "Sensor technologies and microsensor issues for mechatronics systems," *IEEE/ASME Trans. Mechatronics*, vol. 1, no. 1, pp. 39–49, Mar. 1996.

[15] G. A. Bertone, Z. H. Meiksin, and M. L. Carroll, "Investigation of a capacitance-based displacement transducer," *IEEE Trans. Instrum. Meas.*, vol. 39, no. 2, pp. 424–428, Apr. 1990.

[16] N. Yazdi, F. Ayazi, and K. Najafi, "Micromachined inertial sensors," *Proc. IEEE*, vol. 86, no. 8, pp. 1640–1659, Aug. 1998.

[17] G. T. Capraro, A. Farina, H. Griffiths, and M. C. Wicks, "Knowledge-based radar signal and data processing: A tutorial review," *IEEE Signal Process. Mag.*, vol. 23, no. 1, pp. 18–29, Jan. 2006.

[18] M. G. Allen, "Diode laser absorption sensors for gas-dynamic and combustion flows," *Meas. Sci. Technol.*, vol. 9, no. 4, pp. 545–562, Apr. 1998.

[19] S. Donati, L. Falzoni, and S. Merlo, "A PC-interfaced, compact laser-diode feedback interferometer for displacement measurements," *IEEE Trans. Instrum. Meas.*, vol. 45, no. 6, pp. 942–947, Dec. 1996.

[20] S. Donati, G. Giuliani, and S. Merlo, "Laser diode feedback interferometer for measurement of displacements without ambiguity," *IEEE J. Quantum Electron.*, vol. 31, no. 1, pp. 113–119, Jan. 1995.

[21] A. G. Thompson and B. R. Davis, "Optimal linear active suspensions with derivative constraints and output feedback control," *Veh. Syst. Dyn.*, vol. 17, no. 4, pp. 179–192, Jan. 1988.

[22] R. Marino and P. Tomei, "Global adaptive output-feedback control of nonlinear systems. I. Linear parameterization," *IEEE Trans. Autom. Control*, vol. 38, no. 1, pp. 17–32, Jan. 1993.

[23] Y. Y. Zhao and J. Xu, "Effects of delayed feedback control on nonlinear vibration absorber system," *J. Sound Vib.*, vol. 308, no. 1/2, pp. 212–230, Nov. 2007.

[24] N. Olgac and B. T. Holm-Hansen, "A novel active vibration absorption technique: Delayed resonator," *J. Sound. Vib.*, vol. 176, no. 1, pp. 93–104, Sep. 1994.

[25] L. L. Chung, C. C. Lin, and S. Y. Chu, "Optimal direct output feedback of structural control," *J. Eng. Mech.*, vol. 119, no. 11, pp. 2157–2173, Nov. 1993.

[26] J. P. Richard, "Time-delay systems: An overview of some recent advances and open problems," *Automatica*, vol. 39, no. 10, pp. 1667–1694, Oct. 2003.

[27] J. Rodriguez, P. M. Kennel, J. R. Espinoza, M. Trincado, C. A. Silva, and C. A. Rojas, "High-performance control strategies for electrical drives: An experimental assessment," *IEEE Trans. Ind. Electron.*, vol. 59, no. 2, pp. 812–820, Feb. 2012.

[28] C. Y. Chang and H. W. Lie, "Real-time visual tracking and measurement to control fast dynamics of overhand cranes," *IEEE Trans. Ind. Electron.*, vol. 59, no. 3, pp. 1640–1649, Mar. 2012.

[29] H. X. Lin and S. H. Li, "Speed control for PMSM servo system using predictive functional control and extended state observer," *IEEE Trans. Ind. Electron.*, vol. 59, no. 2, pp. 1171–1183, Feb. 2012.

[30] P. B. Schmidt and R. D. Lorenz, "Design principles and implementation of acceleration feedback to improve performance of DC drives," *IEEE Trans. Ind. Appl.*, vol. 28, no. 3, pp. 594–599, May/Jun. 1992.

[31] P. T. Kotnik, S. Yurkovich, and U. Ozguner, "Acceleration feedback for control of a flexible manipulator arm," *J. Robot. Syst.*, vol. 5, no. 3, pp. 181–196, Jun. 2007.

[32] G. D. Hu and T. Mitsui, "Stability analysis of numerical methods for systems of neutral delay-differential equations," *BIT Numer. Math.*, vol. 35, no. 4, pp. 504–515, Dec. 1995.

[33] A. Bellen, N. Guglielmi, and A. E. Ruehli, "Methods for linear systems of circuit delay differential equations of neutral type," *IEEE Trans. Circuits Syst. I, Fundam. Theory Appl.*, vol. 46, no. 1, pp. 201–215, Jan. 1999.

[34] X. L. Luan, S. Peng, and F. Lin, "Stabilization of networked control system with random delay," *IEEE Trans. Ind. Electron.*, vol. 58, no. 9, pp. 4323–4330, Sep. 2011.

[35] M. Lallart, Y. C. Wu, and D. Guyomar, "Switching delay effects on nonlinear piezoelectric energy harvesting techniques," *IEEE Trans. Ind. Electron.*, vol. 59, no. 1, pp. 464–472, Jan. 2012.
[36] A. Carrella, M. J. Brennan, T. P. Waters, and V. Lopes, Jr., "Force and displacement transmissibility of a nonlinear isolator with high-static-low-dynamic-stiffness," *Int. J. Mech. Sci.*, vol. 55, no. 1, pp. 22–29, Feb. 2012.
[37] X. Jiang, D. M. McFarland, L. A. Bergman, and A. F. Vakakis, "Steady state passive nonlinear energy pumping in coupled oscillators: Theoretical and experimental results," *Nonlin. Dyn.*, vol. 33, no. 1, pp. 87–102, Jul. 2003.
[38] I. Kovacic, M. J. Brennan, and B. Lineton, "Effect of a static force on the dynamic behavior of a harmonically excited quasi-zero stiffness system," *J. Sound. Vib.*, vol. 325, no. 4/5, pp. 870–883, Sep. 2009.
[39] T. D. Le and K. K. Ahn, "A vibration isolation system in low frequency excitation region using negative stiffness structure for vehicle seat," *J. Sound. Vib.*, vol. 330, no. 26, pp. 6311–6335, Dec. 2011.

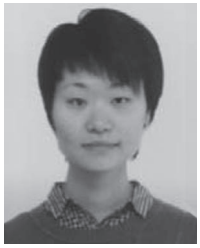

XiuTing Sun was born in Shanghai, China, in August 1987. She received the B.Eng. degree in mechanics in 2009 from Tongji University, Shanghai, China, where she has been working toward the Ph.D. degree since 2009. She has been studying at the Department of Mechanical Engineering, The Hong Kong Polytechnic University, Hong Kong, under a dual degree program since January 2013.

Her research interests include nonlinear isolators.

XingJian Jing (M'13) received the B.S. degree from Zhejiang University, Hangzhou, China, in 1998, the M.S. degree in intelligent systems and control and the Ph.D. degree in mechatronics from the Shenyang Institute of Automation, Chinese Academy of Sciences, Shenyang, China, in 2001 and 2005, respectively, and the Ph.D. degree in nonlinear systems and signal processing from the Department of Automatic Control and Systems Engineering, University of Sheffield, Sheffield, U.K., in 2008.

He is currently an Assistant Professor with the Department of Mechanical Engineering, The Hong Kong Polytechnic University (PolyU), Hong Kong. Before joining PolyU in November 2009, he was a Research Fellow with the Institute of Sound and Vibration Research, University of Southampton, Southampton, U.K., working on biomedical signal processing. His current research interests include nonlinear analysis and design in the frequency domain; system identification, signal processing, and control of complex nonlinear systems; intelligent computing methods; and their applications in nonlinear mechanical systems (sound and vibration control), nonlinear physiological systems (neural systems), robotic systems, etc.

Dr. Jing is an active reviewer for many journals and conferences. He also serves on technical/editorial boards of several international journals/conferences.

Jian Xu was born in Shanghai, China, on December 27, 1961. He received the Ph.D. degree in dynamics and control from Tianjin University, Tianjin, China, in 1994.

Since 2000, he has been a Professor with Tongji University, Shanghai, China, where he is currently the Deputy Dean of the School of Aerospace Engineering and Applied Mechanics. His current research interests include delay-induced dynamics, nonlinear dynamics and control, stability, bifurcation and chaos in nature and engineering, neural networks with delayed connection, and biology systems.

Li Cheng received the B.S. degree in applied mechanics from Xi'an Jiaotong University, Xi'an, China, in 1984 and the DEA and Ph.D. degrees from the Institut National des Sciences Appliquees de Lyon (INSA-Lyon), France, in 1986 and 1989, respectively.

In 1992, he became an Assistant Professor with the Department of Mechanical Engineering, Laval University, Quebec, QC, Canada, where he was later promoted to Associate Professor and then Full Professor. In 2000, he joined the Department of Mechanical Engineering, The Hong Kong Polytechnic University, Hong Kong, where he is currently a Chair Professor and the Director of the Consortium for Sound and Vibration Research. His research interests mainly include noise and vibration control, fluid–structure interaction, damage detection, and smart materials/structures.

Prof. Cheng is a member of the Boards of Directors and committees of several professional organizations, including the Acoustical Society of America, Canadian Acoustical Society, Acoustical Society of China, and Chinese Society of Noise and Vibration Engineering. He also serves on the Editorial Boards or advisory committees for several international journals.